Ion Heating and High-Energy-Particle Production by Ion-Cyclotron Heating in the Large Helical Device

T. Mutoh,[1] R. Kumazawa,[1] T. Seki,[1] T. Watari,[1] K. Saito,[2] Y. Torii,[2] D. A. Hartmann,[3] Y. Zhao,[4] M. Sasao,[1] M. Isobe,[1] M. Osakabe,[1] A. V. Krasilnikov,[5] T. Ozaki,[1] K. Narihara,[1] Y. Nagayama,[1] S. Inagaki,[1] F. Shimpo,[1] G. Nomura,[1] M. Yokota,[1] K. Akaishi,[1] N. Ashikawa,[1] P. de Vries,[1] M. Emoto,[1] H. Funaba,[1] A. Fukuyama,[6] M. Goto,[1] K. Ida,[1] H. Idei,[1] K. Ikeda,[1] N. Inoue,[1] K. Itoh,[1] O. Kaneko,[1] K. Kawahata,[1] S. Kado,[1] A. Komori,[1] T. Kobuchi,[1] S. Kubo,[1] S. Masuzaki,[1] T. Morisaki,[1] S. Morita,[1] J. Miyazawa,[1] S. Murakami,[1] T. Minami,[1] S. Muto,[1] Y. Nakamura,[1] H. Nakanishi,[1] N. Noda,[1] K. Nishimura,[1] K. Ohkubo,[1] N. Ohyabu,[1] S. Ohdachi,[1] Y. Oka,[1] H. Okada,[6] B. J. Peterson,[1] A. Sagara,[1] K. Sato,[1] S. Sakakibara,[1] R. Sakamoto,[1] H. Sasao,[1] M. Sato,[1] T. Shimozuma,[1] M. Shoji,[1] S. Sudo,[1] H. Suzuki,[1] Y. Takeiri,[1] K. Tanaka,[1] K. Toi,[1] T. Tokuzawa,[1] K. Tsumori,[1] K. Y. Watanabe,[1] T. Watanabe,[1] H. Yamada,[1] I. Yamada,[1] S. Yamaguchi,[1] K. Yamazaki,[1] M. Yokoyama,[1] Y. Yoshimura,[1] Y. Hamada,[1] O. Motojima,[1] and M. Fujiwara[1]

[1]*National Institute for Fusion Science, 322-6 Oroshi-cho, Toki, 509-5292 Japan*
[2]*Faculty of Engineering, Nagoya University, Furo-cho, Nagoya, Japan*
[3]*Max-Planck-Institut fuer Plasmaphysik, Euratom Association, D-85748, Garching, Germany*
[4]*Institute of Plasma Physics, Academia Sinica, 230031, Hefei, Anhui, China*
[5]*Troitsk Institute for Innovating and Fusion Research (TRINITI), Troitsk, Russia*
[6]*Kyoto University, Kyoto, Japan*

(Received 11 August 2000)

Ion-cyclotron heating was applied to the Large Helical Device. When the proton-cyclotron resonance was near the saddle point of the magnetic field-strength plane, strong ion-cyclotron damping occurred. Under these conditions efficient plasma heating was achieved for more than one minute. A high-energy ion tail was observed, and the effective tail temperature was determined by a balance between the wave acceleration and the electron-drag relaxation. There was no apparent sign of particle orbit loss effect in the investigated density range of $0.8-1.3 \times 10^{19}$ m^{-3}.

PACS numbers: 52.50.Gj, 52.55.Hc

The Large Helical Device (LHD) is a large heliotron-type device with superconducting windings with a major radius of 3.9 m and a maximum magnetic field on the axis of 3 T [1,2]. The first heating experiment using the ion cyclotron range of frequencies (ICRF) was conducted at a magnetic field of 1.5 T [3,4]. In helical devices, ICRF heating experiments were steadily improved as the device size and the magnetic field strength increased [5–8]. In the LHD experiment in 1999, the magnetic field was raised up to 2.9 T. In this paper the 1999 results of ICRF heating at the magnetic field of 2.9 T are described.

The ICRF heating setup was almost identical to the previous experiment [3,9], while the frequency was raised to 38.5 MHz. This frequency change raised the antenna-coupling resistance from 1 Ω to 3–5 Ω and increased the available heating power to the plasma. A pair of loop antennas was installed at the outer side of the toroid. Near the antenna, the plasma is elongated in the vertical direction, as shown in Fig. 1. Figure 1(a) shows the locations of the resonance and the cutoff layers on a cross section of the toroid where the ICRF antenna is installed. On the cross section, the fundamental cyclotron resonance for protons, the two-ion hybrid resonance, the left-hand cutoff, and the right-hand cutoff are shown. Thin lines show the equimagnetic field strength (equi-B) contours and the magnetic flux surfaces. The upper half of the figure shows the configuration of the best heating results, which occurred on the magnetic field strength for $B = 2.75$ T at the magnetic axis radius of 3.6 m. The lower half of the figure shows the locations of the cyclotron resonance when the resonance moved from $x = -0.32$ to $+0.73$ m as a result of changing the magnetic field strength and the heating frequency. The x coordinate represents the distance from the saddle point of the magnetic field strength, X, shown in the figure. Helical windings are located at the left and right sides on the figure and the magnetic field is strong near the helical windings.

To investigate the heating mechanism of the experiments, a one dimensional (1D) full-wave-analysis code was used [10]. This wave-propagation code includes kinetic effects such as the finite-gyroradius effect and wave/particle interactions. The 1D calculations were performed on the lines perpendicular to the antenna, distributed along the antenna loop on the cross section of Fig. 1(a). Because of the unique equi-B-contour configuration of heliotron devices, the cyclotron damping is very strong for resonance lines located around the saddle point. The reason for this is the large cyclotron-resonance region near the saddle point, which results from the slow change of magnetic field strength. The results of the 1D code calculation are integrated along the antenna loop with a weighting factor for the antenna-current distribution. The power

 0031-9007/00/85(21)/4530(4)$15.00

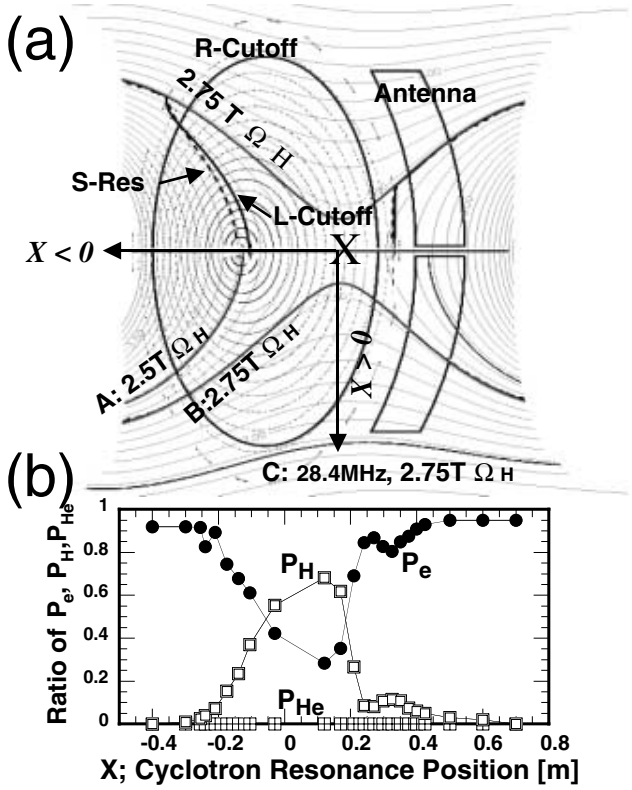

FIG. 1. (a) Right-hand cutoff, R, left-hand cutoff, L, and two-ion hybrid resonance, S, on the cross section of LHD. Frequency = 38.5 MHz (A and B), 28.4 MHz (C), $n_{e0} = 1.5 \times 10^{19}$ m^{-3}, $n_H/n_e = 0.2$. (b) One dimensional full wave code analysis shows the power partition to minority protons, majority helium ions, and electrons by changing the cyclotron resonance position. (Frequency = 38.47 MHz, $k_\parallel = 5$ m^{-1}, $n_{e0} = 1.5 \times 10^{19}$ m^{-3}, $n_H/n_e = 0.2$.)

partitions to the plasma species are shown in Fig. 1(b) for different proton-cyclotron resonance positions. Calculation shows that the minority heating becomes dominant when the cyclotron resonance is located near the saddle point.

ICRF heating was applied to the plasma that was initiated by electron-cyclotron heating (ECH). Figure 2 shows the time evolutions of the plasma parameters for long operation time. The plasma was sustained by ICRF heating for 68 s. The configuration of the resonance and cutoff layers is shown in the upper half of Fig. 1(a). The ICRF power was approximately 0.9 MW, and the stored energy of the plasma was 100–130 kJ. The electron density was approximately 1×10^{19} m^{-3}, and electron and ion temperatures in the core region were approximately 2 keV. The radiation power was almost constant during the ICRF heating. The proton and helium-ion ratio monitored by the Hα and HeI lines was almost constant during the discharge. This long, steady-state plasma sustainment produced by ICRF heating for more than one minute was the first achievement of the ICRF heating of the fusion experimental devices. By increasing the electron density and increasing the input ICRF power up to 1.3 MW, a stored

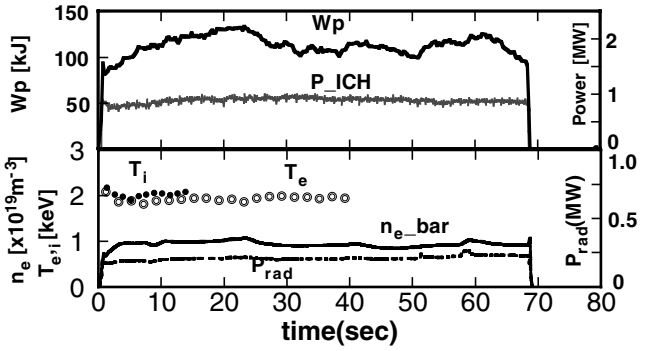

FIG. 2. Time evolutions of diamagnetic stored energy, W_p, line averaged density, electron temperature (Thomson scattering), ion temperature (Ti-XXI Doppler broadening), and radiation loss power of long pulse ICRF discharge (#17170).

energy of 200 kJ was achieved at an electron density of 1.9×10^{19} m^{-3}. This large increase of the stored energy was due to the positive dependence of the energy confinement time on the electron density, $\tau_E \propto n_e^{0.5}$ [2].

The ICRF heating properties depend strongly on the resonance positions. Several plasma properties in the magnetic field range of 2.3–2.9 T and a frequency range of 28.4–38.5 MHz are shown in Fig. 3. The stored energy of the plasma, W_p, for the ICRF sustained mode was plotted by changing the position of the minority ion-cyclotron resonance in Fig. 3(a). The positions *A*, *B*, and *C* are shown in the lower half of Fig. 1(a). The highest performance plasma was achieved at position *B*.

The input power to the plasma was estimated from the differential of W_p immediately after the ICRF was turned

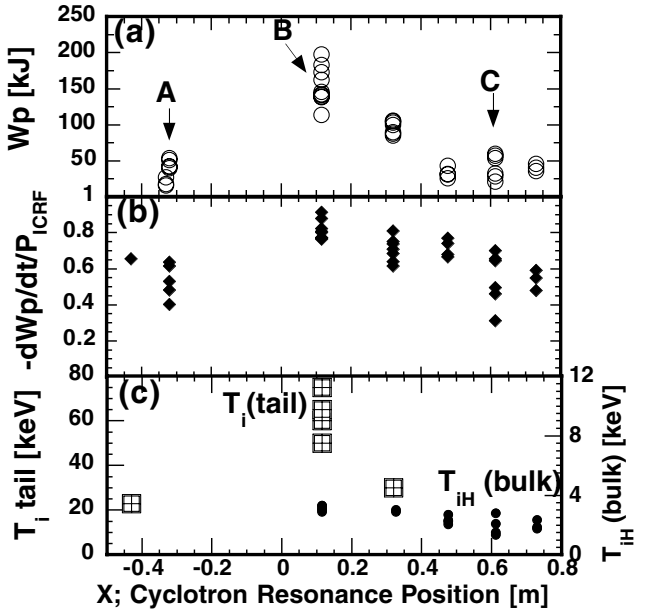

FIG. 3. Heating properties by changing the cyclotron resonance position parameter x. (a) Plasma stored energy, (b) ratio of plasma input power to antenna launched power, and (c) effective tail temperature and bulk temperature of minority protons.

off. The ratios of the input power to the ICRF-launched power are plotted in Fig. 3(b). The efficient power coupling from the antenna to the bulk plasma should occur near position B. However, the power couplings at positions A and C were relatively low. The coupling efficiency depends strongly on the plasma density and the wave damping strength. Both factors were influential in the experiment. The eigenmode signal on the antenna loading resistance at point B was smaller than at other positions for the same plasma density and minority ion concentration. This also means that resonance position B has a larger wave-damping property than other positions.

The bulk proton-energy distribution was measured by a time-of-flight-type neutral-particle analyzer, and the high-energy tail component was measured using a natural diamond detector (NDD) [11] and a silicon diode detector. The minority proton temperature, $T_{i\mathrm{H}}$, and the high-energy tail temperature, T_i(tail), defined over the energy range of 30–110 keV, are plotted in Fig. 3(c). We observed a high-energy tail component near position B. This shows that there is strong cyclotron damping by minority protons on this condition. These data are consistent with the code calculation shown in Fig. 1(b).

In order to study the wave-power transfer to plasma species, the direct electron heating was checked by the time evolution in electron temperature, immediately after turning off the ICRF pulse. Figure 4(a) shows the time evolution of the electron cyclotron emission (ECE) signals at the timing of ICRF turned off. Signals are normalized at the turning-off timing and are classified into three groups of different normalized radius, ρ. For resonance positions A and B, there was no meaningful change of slope in ECE signals; thus most of the wave energy went directly to the ions. Only in the case of position C did a portion of the power go directly to the electrons from the launched wave. For position A, the calculation result of Fig. 1(b) shows that the electron heating is dominant. This disagreement should come from the application of the 1D code which does not include the global mode in the heliotron configuration.

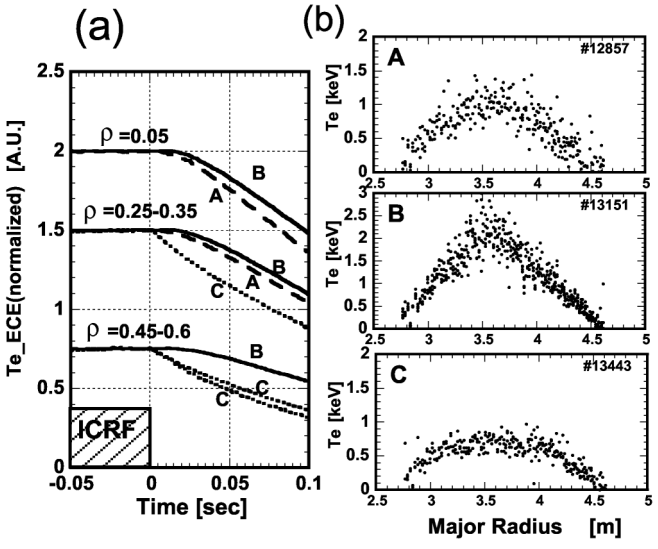

FIG. 4. Time traces of ECE measurement of the several normalized radius positions, ρ, at the ICRF turned off. (b) Electron temperature profiles for the resonance positions of A, B, and C, which are shown in Fig. 1(a).

From the 1D full-wave code, the power to majority helium is negligible. Therefore, the major part of the ICRF power appears to go to the minority protons. In Fig. 4(b) the electron temperature profiles at positions A, B, and C are shown. For A and B there are no signs of direct electron heating in ECE, although a peak in the electron temperature was observed at position B. The reason for the peaked electron-temperature profile is not clear, because the trajectory of the accelerated proton does not cross the magnetic axis region. At least one pitch angle scattering is necessary to reach the axis region. At resonance position C, the mode conversion layer was located at the peripheral region; therefore, a broad electron-temperature profile is reasonable.

At resonance position B, where the minority ion heating was dominant, the apparent high-energy ion tail was observed in neutral-particle energy analyzers. By using the NDD, the time evolution of the effective tail temperature T_i(tail) was measured. In Fig. 5(a) and 5(b), T_i(tail) is shown for two different discharges. Central electron temperature, ICRF input power, and line averaged electron density are also shown. This effective tail temperature was defined for the energy range between 30 and 110 keV. Figure 5(a) shows a discharge sustained by ICRF, and the electron density slowly increasing with the lapse of time. On the other hand, in Fig. 5(b), neutral beam injection (NBI) heating was added to the ICRF-sustained plasma with a stepladder shape, and the electron temperature was changed to follow the total input power. However, the minority proton concentration was barely changed by NBI-injected particles. The change of T_i(tail) depends on electron density, as shown in Fig. 5(a), and on electron temperature as shown in Fig. 5(b).

The velocity-space distribution function for the minority ion can be estimated theoretically from Stix's formula [12]. In the high-energy region, the tail temperature, T_{eff}, approaches the asymptotic value:

$$T_{\mathrm{eff}} \cong T_e(1 + \xi) = T_e \times \left(1 + \frac{\langle P_\perp \rangle t_s}{3nT_e}\right),$$

where ξ is a dimensionless parameter directly proportional to the input power density, $\langle P_\perp \rangle$, and t_s is Spitzer's slowing down time. Finally, T_{eff} is proportional to $\langle P_\perp \rangle T_e^{1.5}/nn_e$. Here n is the minority ion density. This effective temperature is the solution for steady-state balance between the heating acceleration and the electron relaxation.

In Fig. 5(c), the experimentally obtained T_i(tail) for the two discharges are plotted against a parameter that is proportional to the T_{eff}. Here n, $\langle P_\perp \rangle$, and T_e in the

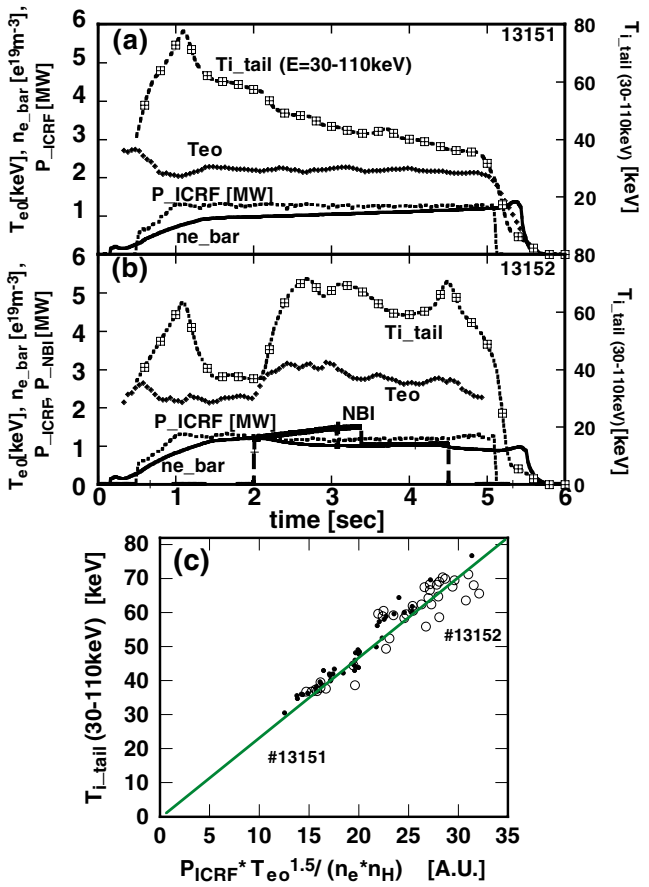

FIG. 5. (a),(b) Time evolutions of high-energy ion tail temperatures of two discharges with electron temperature, density, and input powers. (a) is an ICRF-sustained plasma and (b) is a plasma with additional NBI heating. (c) Tail temperatures of the two discharges are plotted against a parameter proportional to the Stix's effective tail temperature T_{eff}.

above equation are assumed to be proportional to the line-averaged density, input ICRF power, and central electron temperature, respectively. Data during the rising phase of ICRF power were eliminated in order to see the balance at the steady-state condition. The data of the two discharges are in quite good agreement with the solid line, which indicates that the tail temperature is consistent with Stix's formula.

This agreement supports the proposition that the wave-induced proton distribution is entirely balanced by the electron drag on the two discharges. High-energy particles with energies up to 300 keV were observed in the higher horizontal-axis region, where the input power is large, the electron temperature is high, and the accelerated-particle density is small. The growth rate of the tail temperature does not show any saturation tendency, suggesting that ICRF power produces no particle orbit-loss effects for highly accelerated ions in the perpendicular direction. In addition, the stored energy of the plasma was proportional to the input ICRF power for a density range of over 0.8×10^{19} m^{-3}. These data also supported the premise that the particle-loss effect was negligibly small.

In summary, an efficient plasma heating and maintenance for more than one minute was achieved by ICRF heating in the LHD. This is the first achievement in fusion experimental devices. Ions were mainly heated by waves and a high-energy ion tail was observed. These results are consistent with 1D full-wave-analysis-code calculation. Strong ion cyclotron damping could be attributed to the saddle-shaped magnetic-field configuration of the heliotron device. The balance of the wave heating and the electron drag determined the high-energy tail temperature, and there is no sign of fast-ion loss for the energy range up to 300 keV. This is the first evidence of good confinement of high-energy particles having large pitch angle in velocity space in the heliotron device.

The authors thank Professor A. Iiyoshi and the staff of the LHD project.

[1] M. Fujiwara *et al.,* Plasma Phys. Controlled Fusion **41**, B157 (1999).
[2] O. Motojima *et al.,* Phys. Plasmas **6**, 1843 (1999).
[3] T. Mutoh *et al.,* Plasma Phys. Controlled Fusion **42**, 265 (2000).
[4] R. Kumazawa *et al.,* in *Proceedings of the 13th APS Topical Conference on Applications of Radio Frequency Power to Plasmas, Annapolis, MD, 1999,* edited by S. Bernabei and Franco Paoletti (American Institute of Physics, Melville, NY, 1999), p. 160.
[5] T. Mutoh *et al.,* Nucl. Fusion **24**, 1003 (1984).
[6] S. Masuda *et al.,* Nucl. Fusion **37**, 53 (1997).
[7] D. A. Hartmann *et al.,* in *Fusion Energy 1998, Proceedings of the 17th Conference, Yokohama, Japan* (International Atomic Energy Agency, Vienna, 1999), Vol. 2, p. 575.
[8] T. Watari, Plasma Phys. Controlled Fusion **40**, A13 (1998).
[9] T. Seki *et al.,* J. Plasma Fusion Res. (to be published).
[10] A. Fukuyama *et al.,* Nucl. Fusion **23**, 1005 (1983).
[11] A. V. Krasilnikov *et al.,* Nucl. Fusion **39**, 1111 (1999).
[12] T. H. Stix, *Waves in Plasmas* (American Institute of Physics, New York, 1992), p. 512.